

Tuning Plasmonic Enhancement of Single Nanocrystal Upconversion Luminescence by Varying Gold Nanorod Diameter

Yingxian Xue, Chengjie Ding, Youying Rong, Qiang Ma, Chengda Pan, E Wu, Botao Wu,* and Heping Zeng*

Plasmonic enhancement induced by metallic nanostructures is an effective strategy to improve the upconversion efficiency of lanthanide-doped nanocrystals. It is demonstrated that plasmonic enhancement of the upconversion luminescence (UCL) of single $\text{NaYF}_4:\text{Yb}^{3+}/\text{Er}^{3+}/\text{Mn}^{2+}$ nanocrystal can be tuned by tailoring scattering and absorption cross sections of gold nanorods, which is synthesized wet chemically. The assembly of the single gold nanorod and single upconversion nanocrystal is achieved by the atomic force microscope probe manipulation. By selecting two kinds of gold nanorods with similar longitudinal surface plasmon resonance wavelength but different diameters (27.3 and 46.7 nm), which extinction spectra are separately dominant by the absorption and scattering, the maximum UCL enhancement by a factor of 110 is achieved with the 46.7 nm-diameter gold nanorod, while it is 19 for the nanorod with the diameter of 27.3 nm. Such strong enhancement with the larger gold nanorod is due to stronger scattering ability and greater extent of the near-field enhancement. The enhanced UCL shows a strong dependence on the excitation polarization relative to the nanorod long axis. Time-resolved measurements and finite-difference time-domain simulations unveil that both excitation and emission processes of UCL are accelerated by the nanorod plasmonic effect.

1. Introduction

Lanthanide-doped upconversion nanoparticles (UCNPs) belong to an attractive class of nanomaterials with the ability to emitting in the ultraviolet and visible region upon

excitation with a near-infrared or infrared radiation by a process known as photon upconversion.^[1–3] Compared with conventional organic fluorophores and semiconducting nanocrystals, lanthanide-doped UCNPs possess excellent chemical and spectral properties, such as low toxicity, high thermal/photostability, high resistance to photobleaching, narrow and tunable emission bandwidths, long emission lifetime, and large anti-Stokes shifts.^[4,5] Therefore, lanthanide-doped UCNPs show great potential in a variety of possible applications including biological labeling and imaging,^[6,7] photodynamic therapy,^[8,9] photovoltaics,^[10] and display technologies.^[11] However, UCNPs usually suffer from low upconversion emission efficiency owing to the small absorption cross sections induced by the forbidden transitions between 4f orbitals of the lanthanide dopants. For example, the quantum yield of the extensively studied $\beta\text{-NaYF}_4$ nanocrystals codoped with Yb^{3+} and Er^{3+} is usually below 1%.^[12]

Y. Xue, C. Ding, Y. Rong, Q. Ma, C. Pan, Prof. E. Wu,
Dr. B. Wu, Prof. H. Zeng
State Key Laboratory of Precision Spectroscopy
East China Normal University
Shanghai 20006 2, China
E-mail: btwu@phy.ecnu.edu.cn;
hpzeng@phy.ecnu.edu.cn



The ORCID identification number(s) for the author(s) of this article can be found under <https://doi.org/10.1002/sml.201701155>.

DOI: 10.1002/sml.201701155

And efforts were made to develop novel $\text{LiLuF}_4:\text{Ln}^{3+}$ UCNP with typically high absolute upconversion quantum yields up to 5.0% and 7.6% for Er^{3+} and Tm^{3+} , respectively.^[13] For widespread applications, the UCNP's efficiency needs to be improved further.

On one hand, a few efforts have been made to enhance the upconversion luminescence (UCL) of UCNP by developing design strategies for UCNP.^[4,14,15] On the other hand, plasmonic metallic nanostructures are introduced to enhance the UCL. The collective oscillation of conduction electrons on metallic nanostructure surfaces when interacting with incident light, known as surface plasmon resonance, can produce strong field localization in subwavelength scale in the vicinity of the metallic nanostructures. This localization results in the near-field enhancement by orders of magnitude and can be used to greatly promote photochemical reactions^[16,17] and amplify the luminescence from nearby optical emitters as extensively demonstrated in plasmonic-enhanced fluorescence of semiconductor quantum dots and dye molecules.^[18–22] This strategy has also been extended to enhance the UCL of UCNP with metallic nanoparticles,^[23–33] structured metallic surfaces,^[34–39] metal shell architectures,^[40–43] and metallic tip.^[44,45]

Gold nanorods exhibit transverse and longitudinal surface plasmon resonances (LSPRs) that correspond to electron oscillations perpendicular and parallel to the rod long axis direction, respectively. One of the most intriguing properties of Au nanorods is that their LSPR depends strongly on the nanorod aspect ratio, and can be systematically tuned from visible to infrared regions.^[46–48] Furthermore, the scattering and the absorption cross sections of Au nanorods at a given LSPR wavelength are largely determined by their diameters.^[47] Therefore, the diameter of Au nanorods is a crucial factor for their applications. For Au nanorods with diameter larger than 30 nm, extinction is dominated by scattering, making them favorable for applications in metal-enhanced fluorescence and bioimaging,^[20,21,49] and so forth, whereas for smaller Au nanorods, absorption mainly contributes to extinction, which makes them suitable for photothermal therapy with a high photon-to-heat conversion efficiency.^[50,51] Recent reports also demonstrated the plasmonic enhancement UCL of UCNP by single or assembly Au nanorods.^[25–33] However, the diameters of Au nanorods used in these works are all below 30 nm, and therefore the enhancement efficiency of these Au nanorods will be reduced due to the photon-to-heat conversion loss. And the previous work mostly concentrated on the tuning of LSPR positions and controlling the distance between gold nanorods and fluorescence emitters. The experiment exploring the effect of tuning the scattering/absorption ratio of gold nanorods on their enhancement efficiency is seldom reported. Here, the experimental ability to improve the enhancement efficiency on the UCL of UCNP by tuning the scattering and absorption cross-sections of Au nanorods at a given LSPR wavelength is explored. Single UCNP was manipulated to separately couple with single Au nanorods of two diameters (27.3 and 46.7 nm) by an atomic force microscope (AFM) probe, which extinction spectra were dominated by the absorption and scattering, respectively. UCL properties of single UCNP–Au nanorod hybrid

dimer under the excitation of 980 nm laser were examined by single-particle spectroscopy on a scanning confocal microscopy. A maximum UCL enhancement of 110 times was obtained in Au nanorod with the 46.7 nm diameter, and the enhancement factor was 19 with the smaller one. Rise and decay time measurements reveal that both the excitation and emission processes were accelerated by the plasmonic near field around Au nanorod tips.

2. Results and Discussion

The UCNP used here were Yb^{3+} , Er^{3+} , and Mn^{2+} co-doped NaYF_4 nanocrystals coated with a silica shell. **Figure 1a** shows the X-ray diffraction (XRD) pattern of the UCNP, and all the peaks can be well indexed by hexagonal phase NaYF_4 crystals (JCPDS file No. 16-0334), providing the evidence of the pure hexagonal phase of the UCNP. Representative transmission electron microscope (TEM) image of the UCNP is shown in **Figure 1b**. The UCNP have a truncated-corner square shape and average size of about 35.6 nm with the silica shell thickness of about 7 nm. Actually, the homogeneous coating with the similar composition as the UCNP host (e.g., NaYF_4) could also be used to enhance the UCL. However, the optimal NaYF_4 coating thickness is usually ≈ 3 nm, which corresponds to the critical distance of shielding the interaction between the lanthanides and surface defects or solvent molecules in the surrounding environment.^[52] Further increasing the coating thickness does not lead to the steady enhancement in the UCL. Meanwhile, the coating thickness is difficult to be identified by the conventional TEM analyses because of similar lattice and very weak contrast between the UCNP host and coating material.^[53] In order to prevent the energy transfer between UCNP and Au nanorod, the spacer thickness between them should be larger (about 7 nm in our case). The amorphous SiO_2 coating on NaYF_4 nanocrystals can also improve the UCL, but the enhancement is very weak because amorphous SiO_2 cannot provide strong crystal field like NaYF_4 coating. As a spacer between the UCNP and Au nanorod, the thickness of the SiO_2 coating could be finely controlled and easily identified by TEM analyses. Therefore, we chose the UCNP with SiO_2 coating. In previous experimental reports, the optimized separation distance between UCNP and Au nanoparticles was revealed to be around 6 to 10 nm.^[24,25,27] The 7 nm silica layer could prevent Au nanorods from approaching too close to UCNP and quench the UCL. At the same time the high UCL enhancement could be achieved. High-resolution transmission electron microscope (HRTEM) image with crystal lattice in **Figure 1c** gives an adjacent lattice fringe distance of 0.310 nm, which can be assigned to the (110) crystal plane of the hexagonal phase NaYF_4 . The UCL spectrum of single UCNP was characterized under the excitation of 980 nm laser. An intense red emission band around 660 nm and a very weak green emission band ≈ 550 nm could be identified in the spectrum as shown in **Figure 1d**, which were attributed to the $^4\text{F}_{9/2} \rightarrow ^4\text{I}_{15/2}$ and the $^2\text{H}_{11/2}, ^4\text{S}_{3/2} \rightarrow ^4\text{I}_{15/2}$ transitions of Er^{3+} ion (**Figure 1e**), respectively. Many previous studies on the plasmonic enhancement UCL of Yb^{3+} and Er^{3+}

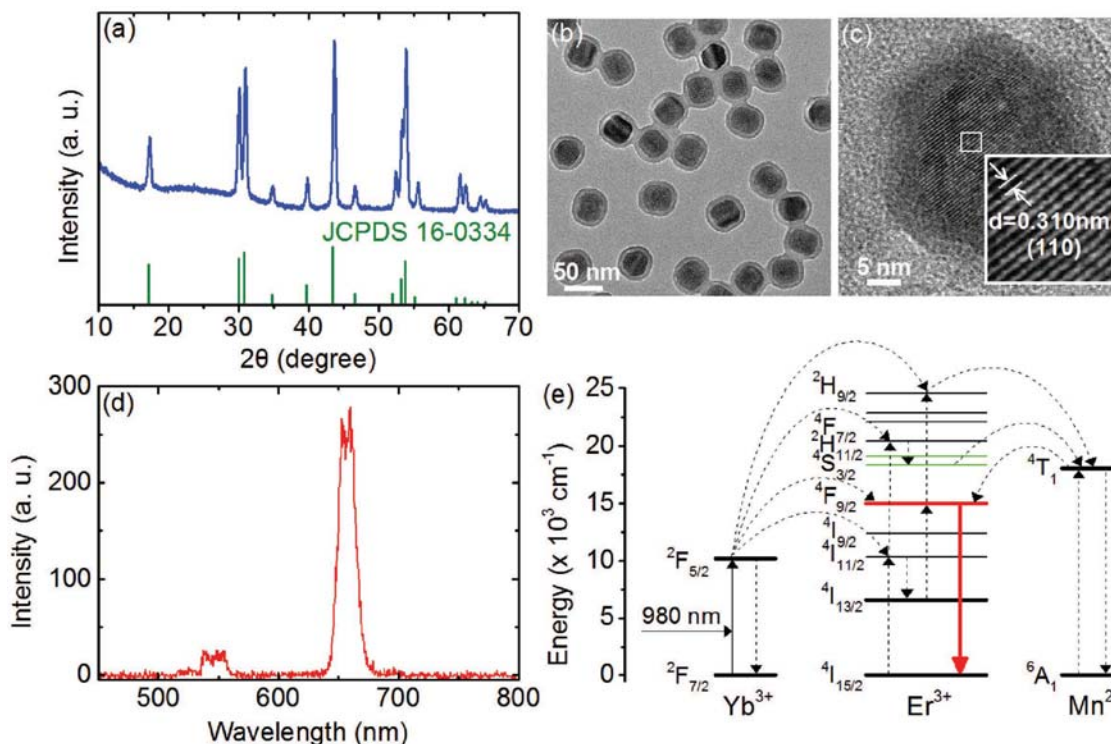


Figure 1. a) XRD pattern of the UCNPs. b) Low-resolution TEM image of the UCNPs. c) High-resolution TEM image of the UCNPs with characteristic lattice plane information. d) Upconversion luminescent spectrum of a single UCNP excited by 980 nm laser. e) Energy level diagram with the possible upconversion transitions of Yb³⁺/Er³⁺/Mn²⁺ co-doped NaYF₄ nanocrystals.

coactivated hexagonal NaYF₄ nanocrystals have indicated that the enhancement factor was not equal for green and red emissions but varied strongly with different characteristics of plasmonic structures.^[23–37,41,42,44,45] Furthermore, a fraction of red UCL in Yb³⁺/Er³⁺ codoped NaYF₄ nanocrystals originates from the excited state nonradiative relaxation of the green UCL (⁴S_{3/2} level).^[24,36,37,44,45] Therefore, to assess the plasmonic enhancement effectiveness of Au nanorods with different diameters quantitatively as well as to exclude the disturbance of the nonradiative relaxation between the excited states of green and red emissions, Yb³⁺/Er³⁺/Mn²⁺ codoped NaYF₄ nanocrystals were chosen. Mn²⁺ ions could disturb the transition possibilities between the green and the red emissions of Er³⁺ by nonradiative energy transfer from the ²H_{11/2} and ⁴S_{3/2} levels of Er³⁺ to the ⁴T₁ level of Mn²⁺, followed by back-energy transfer to the ⁴F_{9/2} level of Er³⁺ (Figure 1e).^[54]

Au nanorods of two diameters with the similar LSPR wavelength were synthesized by colloid seed growth method.^[48] Figure 2a–c exhibits their extinction spectra (not scaled relative to the nanorod concentration) in water solutions and representative TEM images. It is notable that these two kinds of Au nanorods showed the same LSPR wavelength at about 708 nm, and the average diameters were 27.3 ± 1.7 nm and 46.7 ± 5.3 nm, while the average lengths were 78.1 ± 8.2 nm and 115.7 ± 13.1 nm, respectively. Meanwhile, the simulated extinction, absorption, and scattering spectra using the average sizes of the Au nanorods are shown in Figure 2d,e. The corresponding LSPR wavelengths of the Au nanorods deposited on the glass substrate

in air all shifted to about 660 nm, matching the red emission wavelength of the UCNPs. The blue shift in the LSPR wavelengths of Au nanorods is due to the refractive index decrease of the medium surrounding Au nanorods changed from water to glass in air. It has been known that a reduction in the refractive index of surrounding medium causes a blue shift of the plasmonic peak of noble metal nanoparticles.^[55] We also performed dark-field image and scattering spectrum measurements for single Au nanorods as shown in Figure 3. Figure 3a,b exhibits representative dark-field images for single Au nanorods with the diameters of 27.3 and 46.7 nm, respectively, and scattering spectra of single Au nanorods for the two samples are shown in Figure 3c,d. Comparing with the ensemble extinction spectra of Au nanorods in aqueous solution in Figure 2a, these single nanorod scattering spectra become narrow and have a clear blue shift, which is consistent with the simulation results in Figure 2d,e. As mentioned above, this blue shift is due to the refractive index decrease of the surrounding medium when Au nanorods dispersed in aqueous solution were deposited on glass substrates in air.

The controlled coupling between the single UCNP and the single Au nanorod as well as the UCL properties of the single UCNP without and with single Au nanorod was conducted on the combined system of a scanning confocal microscope and an AFM, which schematic diagram is shown in Figure S1 (Supporting Information). Manipulation of individual nanoparticles by an AFM probe is a powerful and highly advantageous method to self-assemble predesigned structures with controlled orientation.^[23,56,57] At first, UCNPs

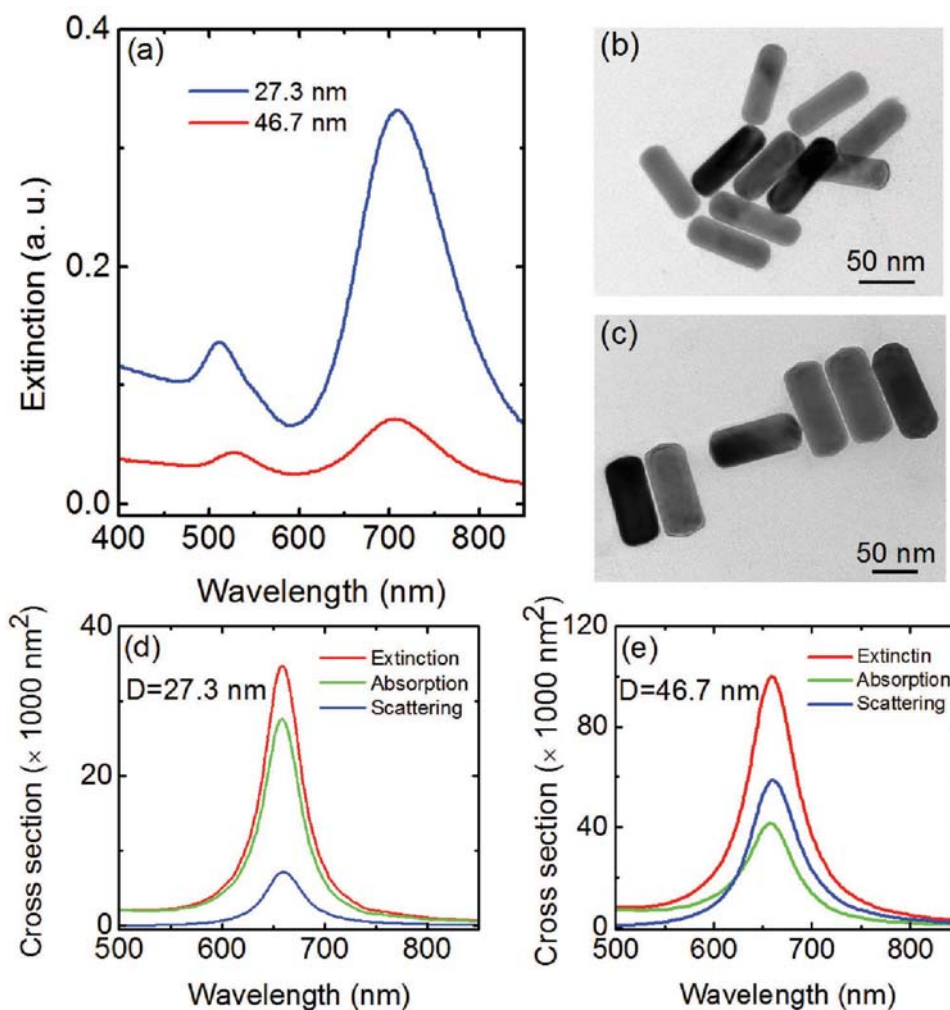


Figure 2. a) Extinction spectra of Au nanorods with the diameters of 27.3 and 46.7 nm in aqueous solution (not scaled relative to the nanorods concentrations). b,c) TEM images of Au nanorods with the diameters of 27.3 and 46.7 nm, respectively. d,e) Simulated extinction, absorption and scattering spectra of Au nanorods with the diameters of 27.3 and 46.7 nm, respectively.

and Au nanorods in an appropriate particle density were deposited on a very smooth glass substrate with a surface roughness below 0.8 nm one after another by the spin-coating method. Then the AFM was operated in tapping mode to image and identify the location of the single UCNP and the single Au nanorod in proximity. Next, the AFM probe pushed the UCNP in contact mode toward to one tip of the Au nanorod to construct the UCNP–Au nanorod hybrid dimer. To demonstrate the assemble process intuitively, representative 3D AFM images for Au nanorods with the diameters of 27.3 and 46.7 nm at different assembling stages are shown in **Figure 4a,b**, respectively. And **Figure 4c,d** shows the cross-section analyses along the axis direction of the hybrid dimers (indicated by green lines in the insets of **Figure 4c,d**). The heights of the UCNPs and Au nanorods are in good agreement with the TEM images. AFM images and cross-section analyses of the additional UCNP–Au nanorod hybrid dimers are presented in **Figure S2** (Supporting Information).

UCL of single UCNPs and the UCNP–Au nanorod hybrid dimers was studied by the scanning confocal microscope depicted in **Figure S1** (Supporting Information). The 980 nm laser power density was maintained at about $4.4 \times 10^5 \text{ W cm}^{-2}$

during the measurement. A half-wave plate at the output of the laser allowed us to rotate the laser linear polarization direction. UCL spectra of single UCNPs before and after assembling with single Au nanorods under transverse (\perp) and longitudinal (\parallel) polarized laser excitations relative to the long axis of Au nanorod are exhibited in **Figure 5a,b**. As expected, the single UCNP without Au nanorods shows little sensitivity to the laser polarization (**Figure S3a,c**, Supporting Information). However, for the UCNP–Au nanorod hybrid dimers, the UCL intensity shows a maximum or minimum for the longitudinal or transverse laser polarization (**Figure S3b,d**, Supporting Information), but they are all significantly larger than the single UCNP luminescence intensity. Importantly, for the longitudinal polarization, the presence of Au nanorod with the diameter of 46.7 nm is found to enhance the UCL intensity by a factor of 110, while the enhancement factor is only about 19 for the case of Au nanorod with the diameter of 27.3 nm. The enhancement factor was obtained according to at least five repeated measurements. This significant UCL enhancement achieved in the larger diameter Au nanorod is ascribed to its larger scattering cross-section and near-field enhancement. UCL measurements were also performed on several

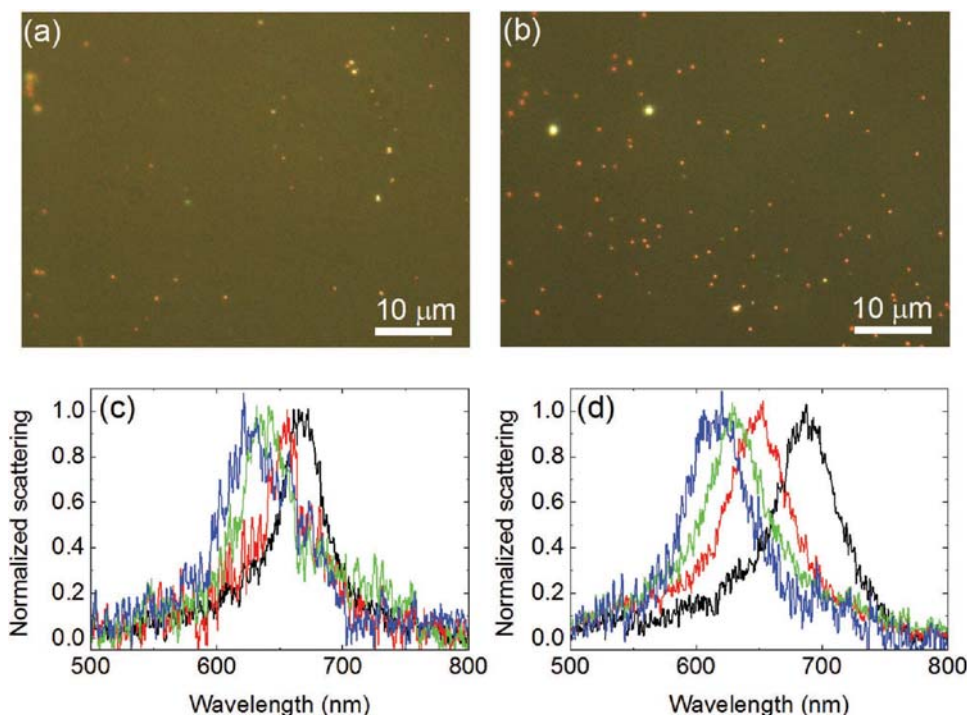


Figure 3. a,b) Dark-filed scattering images of Au nanorods with the diameters of 27.3 and 46.7 nm, respectively. The exposure times for the two Au nanorod samples are separately 0.5 and 0.1 s. c,d) Normalized scattering spectra of single Au nanorods taken from (a) and (b), respectively, showing a rod-to-rod variation of LSPR wavelengths.

examples for each diameter of Au nanorods (Figure S4a, Supporting Information). The UCL intensity for different single UCNPs shows little variation, while large fluctuation in intensity was observed when the UCNPs were coupled with different Au nanorods, especially for the longitudinal polarization. The enhancement factor in the longitudinal polarization for Au nanorods with the diameters of 27.3 nm varied from 7.9 to 19.0, while it changed from 25.3 to 110.0 for Au nanorods with the 46.7 nm diameter (Figure S4b, Supporting Information). The variation of enhancement factors for different samples was due to the dispersibility in Au nanorod sizes, which results in the variation of LSPR wavelengths and electromagnetic near-field around Au nanorods. It is known that UCL intensity I exhibits distinct power law dependence on the excitation power density P : $I \propto P^n$, where n is the number of pump photons required to excite electrons to an emitting state. The slope of the UCL intensity versus the excitation power density plotted in a double-logarithmic diagram represents the photon number involved in the energy transfer process. We measured the UCL intensity at 660 nm for the single UCNPs and hybrid dimers in Figure 4a,b as a function of the laser power density and plotted in a double-logarithmic diagram, as shown in Figure 5c,d. The slope for each structure was analyzed by a linear fitting. For both single UCNP and the hybrid dimer, the UCL intensity exhibits quadratic and linear dependences on the excitation power density at low and high laser power density, respectively, which follows the previous reports.^[24,28,37] The exception is that the transition between the weak and strong excitation regimes shifted to lower power density for the UCNP–Au nanorod hybrid dimers. This result clearly shows that the LSPR of

Au nanorods enhanced the local electric field density. It also indicates that the upconversion process was dominated by a two-photon energy transfer mechanism with negligible contributions of a three-photon process.

To analyze the effect of the LSPR of Au nanorods on the upconversion process of the UCNPs, we performed time-resolved UCL measurements on the single UCNP before and after assembling with Au nanorods. **Figure 6** shows the rise and decay times for the single nanocrystals and hybrid dimers in longitudinal and transverse polarizations. Obviously, the rise and decay times are all decreased when the UCNPs are coupled with the Au nanorods, and reach the shortest for the longitudinal polarization. The decrease of the decay times of the UCNPs coupled with Au nanorods might be caused by the increased radiative rate of the UCNPs, the energy transfer rate from UCNPs to Au nanorods and the local thermal effect of Au nanorods under the illumination of laser.^[24,37,38] However, the 7 nm SiO₂ shell on the UCNPs could largely hinder the energy transfer from UCNP to Au nanorod, thus the energy transfer between UCNP and Au nanorod would be very small. Moreover, since the excitation power density used in the time-resolved measurement is below the power density range of saturation effect (the lower portions in Figure 5c,d), in which the local thermal effect might happen,^[38] the thermal effect can be ruled out. Therefore, the decrease of the decay times of the UCNPs could be mainly attributed to an increase in the radiative rates of the UCNPs induced by the electromagnetic coupling between the UCNPs and Au nanorods. And the decrease in the rise times could be explained by the absorption enhancement of UCNPs to the 980 nm pump laser by the Au nanorods, which

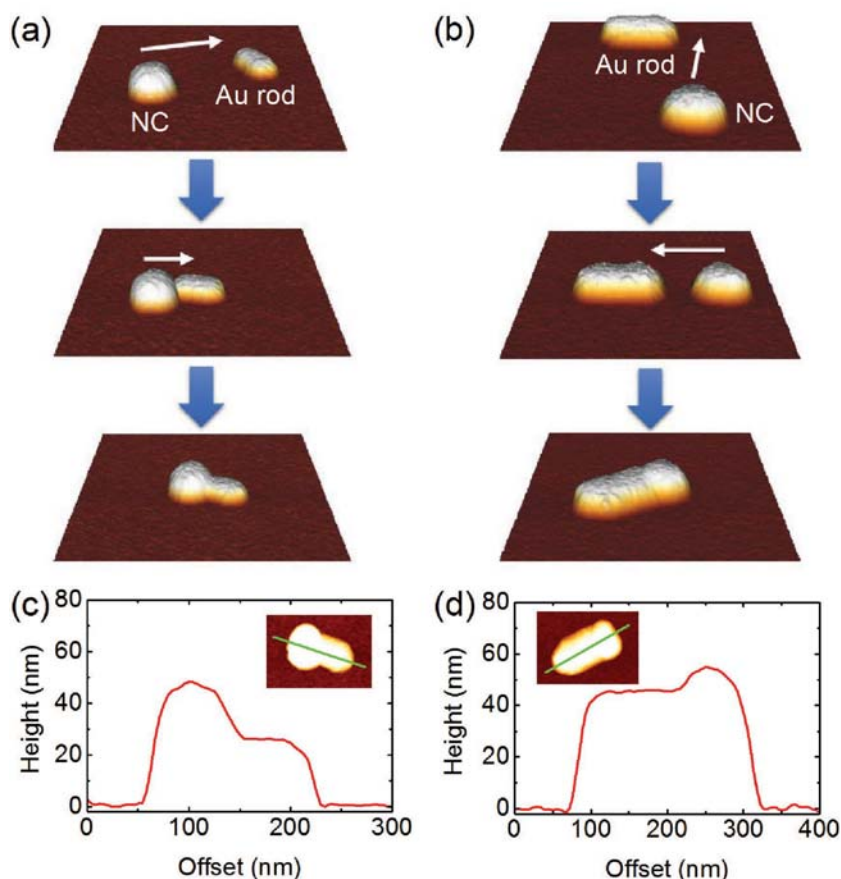


Figure 4. a,b) Representative 3D AFM images for Au nanorods with the diameters of 27.3 and 46.7 nm at different assembling stages, and white arrows indicate the assembly direction. NC: nanocrystal. c,d) Corresponding cross-section analyses along the axis direction of the UCNP–Au nanorod hybrid dimers (indicated by green lines in the insets).

was caused by the nonresonant enhancement of the pump excitation field accompanied by a faster excitation rate of Yb^{3+} ions and energy transfer rate of Yb^{3+} to Er^{3+} ions.^[24,36] The time-resolved UCL results indicate that the excitation and emission processes of UCNPs as well as the energy transfer process of Yb^{3+} to Er^{3+} ions were all influenced by the LSPR of Au nanorods.

To better understand the enhancement magnitude and sample-to-sample variation of UCL enhancement in the UCNP–Au nanorod hybrid dimers, dark-field measurements for single Au nanorods and theoretical simulations were performed. The dark-field images and scattering spectrum are shown in the above Figure 3. The first impression from the dark-field images in Figure 3a,b is that the larger Au nanorods were brighter than the smaller ones in scattering intensity, although the exposure time for the larger Au nanorods (0.5 s) was half of that for the smaller ones (1 s). According to the simulation results in Figure 2d,e, the scattering intensity of the larger nanorod was eight times that of the smaller one, while the extinction intensity was only increased by 2.9 times, clearly indicating the tuning of the relative contributions of scattering and absorption to extinction of Au nanorods with similar LSPR by varying their diameters. Figure 3c,d indicates that the LSPR peak

wavelengths varied among different single Au nanorods due to the difference in nanorod size.^[47,48] It can be expected that Au nanorods with the LSPR wavelengths matching the red emission of the UCNPs will give a stronger UCL enhancement, which means that the UCL enhancement factor will vary due to the polydispersity in Au nanorod sizes, in consistency with the experimental results.

Theoretical simulations based on finite-difference time-domain (FDTD) method were performed as well. The transverse polarization produces a smaller UCL enhancement compared with the longitudinal polarization (Figure 5a,b), thus the simulations only work on the longitudinal polarization. UCL enhancement arises from both excitation enhancement η_{exc} and quantum efficiency enhancement Q . During the excitation process, the incident 980 nm laser excites not only the UCNPs but also the LSPR of Au nanorods. The LSPR produces enhanced local near-field and increases excitation rate. The excitation enhancement η_{exc} is proportional to the local near-field enhancement $|E|^2/|E_0|^2$. In the subsequent emission process, the presence of Au nanorods alters the quantum efficiency of UCNPs via the modification of both radiative and nonradiative decay rates. The initial quantum efficiency q_0 of the UCNPs can

be expressed as $q_0 = \frac{K_r^0}{K_r^0 + K_{nr}^0}$, where K_r^0

and K_{nr}^0 are the initial radiative and nonradiative decay rates of the UCNPs without Au nanorods, respectively. When assembled with Au nanorods, the quantum efficiency q of the UCNPs is defined as:

$$q = \frac{K_r}{K_r + K_{nr} + K_{et}} \quad (1)$$

where K_r , K_{nr} , and K_{et} are the radiative rate, nonradiative decay rate, and energy transfer rate between the UCNPs and Au nanorods, respectively.^[58,59] Therefore, the quantum efficiency enhancement can be written as:

$$Q = \frac{q}{q_0} = \frac{K_r}{K_r^0} \times \frac{K_r^0 + K_{nr}^0}{K_r + K_{nr} + K_{et}} \quad (2)$$

The nonradiative decay rate, which is determined by the crystallinity, surface termination, etc. of the UCNPs, can be reasonably assumed to be not affected by the electromagnetic environment induced by Au nanorods, thus we have $K_{nr} \approx K_{nr}^0$. Since the quantum efficiency of the UCNPs is very low, we have $K_{nr} \gg K_r > K_r^0$. In addition, $K_{nr}^0 \gg K_{et}$ because the silica shell of about 7 nm around the UCNPs can effectively prevent the energy transfer between the UCNPs and

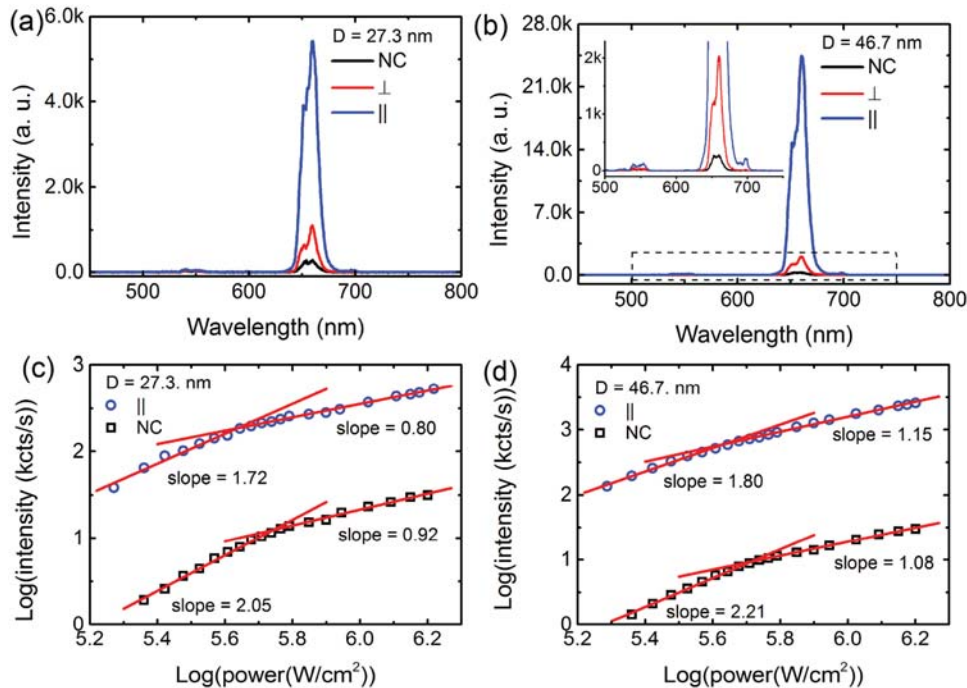


Figure 5. a,b) UCL spectra of single nanocrystals (NCs) before and after assembling with single Au nanorods with the diameters of 27.3 and 46.7 nm under transverse (⊥) and longitudinal (∥) polarized laser excitations. Excitation power density was about $4.4 \times 10^5 \text{ W cm}^{-2}$. The inset in (b) shows the UCL spectra with a small intensity scale. c,d) UCL intensity dependent on the excitation power density for single NCs and UCNP–Au nanorod dimers with the diameters of 27.3 and 46.7 nm in the longitudinal (∥) polarized laser excitation.

Au nanorods. Therefore, the quantum efficiency enhancement Q can be expressed as:

$$Q \approx \frac{K_r}{K_r^0} \quad (3)$$

After the series of reasonable transforms, the overall UCL enhancement F , which is the product of the excitation enhancement and quantum efficiency enhancement, can be simplified to a commonly used form:^[60]

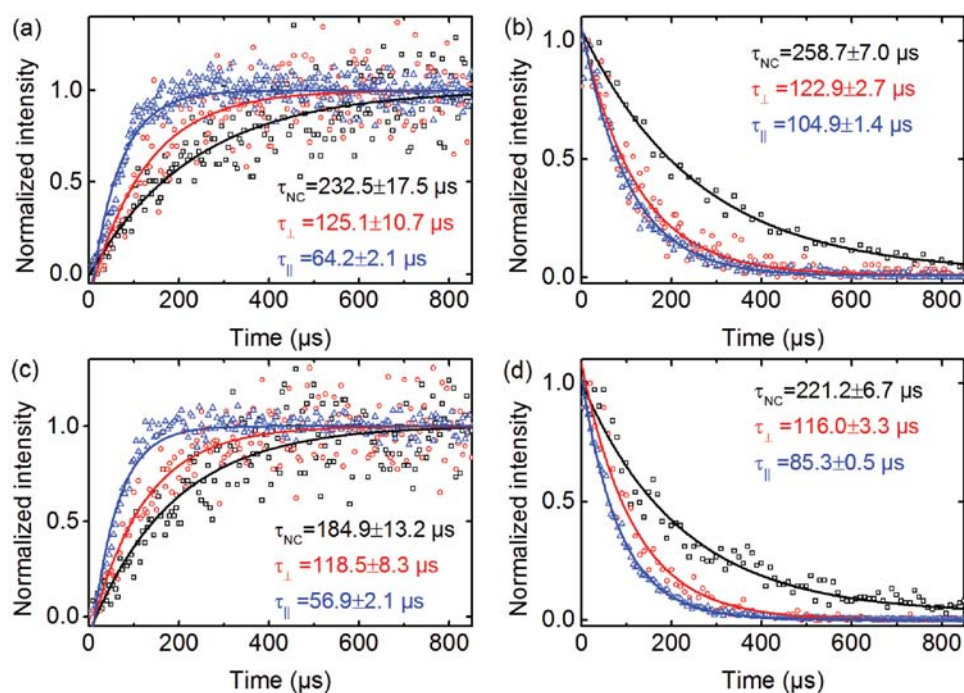


Figure 6. a,b) Rising and decay times for the single nanocrystals (NCs) and UCNP–Au nanorod (the diameter of 27.3 nm) hybrid dimers in longitudinal and transverse polarizations. c,d) Au nanorod with the diameter of 46.7 nm.

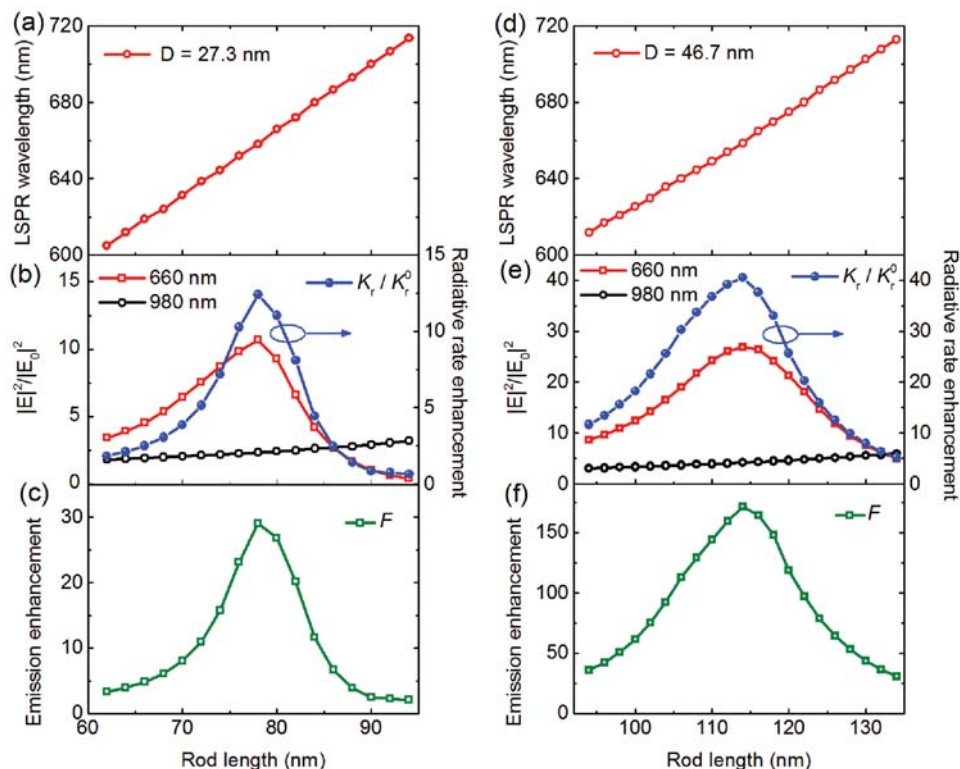


Figure 7. a–c) Simulated LSPR wavelengths, near-field enhancements at 660 and 980 nm in the center position of UCNP (25 nm away from the nanorod’s tip) and radiative rate enhancement K_r/K_r^0 as well as the overall emission enhancement F as a function of rod length for Au nanorods with the diameter of 27.3 nm. d–f) those for Au nanorods with the diameter of 46.7 nm. In (b) and (c), the distance between the point dipole source and the nanorod’s tip is also 25 nm for the radiative rate enhancement simulation.

$$F = \eta_{\text{exc}} \times Q \approx \frac{|E|^2}{|E_0|^2} \times \frac{K_r}{K_r^0} \quad (4)$$

Using the FDTD Solutions software, we simulated the LSPR wavelength and near-field enhancements at 980 and 660 nm as well as radiative rate enhancement as a function of rod length for Au nanorods with the diameters of 27.3 and 46.7 nm, respectively, and the results are shown in **Figure 7a,b,d,e**. It can be seen that the LSPR wavelength of Au nanorod shows a linear dependence with the tuning of nanorod length, in agreement with the previous experimental report.^[47] The LSPR wavelengths match the red emission of UCNPs when the rod lengths are 78 and 116 nm for the Au nanorods with the diameters of 27.3 and 46.7 nm, respectively (Figure 7a,d). For Au nanorods with a constant diameter, the excitation enhancement at the excitation wavelength of 980 nm almost increases linearly with increasing rod length, while the near-field enhancement at the emission wavelength of 660 nm reaches the largest when the rod length is 78 or 116 nm, where the LSPR wavelength matches the emission wavelength of 660 nm, as shown in Figure 7b,e. Meanwhile, for the larger Au nanorod, the near-field enhancements at 980 and 660 nm are higher than that of the smaller Au nanorod at a given LSPR wavelength due to the stronger scattering ability of the larger Au nanorod, as seen in Figure 3a,b.

The radiative rate enhancement K_r/K_r^0 was calculated as a function of rod length. The results are also exhibited in Figure 7b,e. Obviously, for the nanorods with a constant

diameter, the radiative rate enhancement strongly depends on the rod length and is maximum for the rod when its LSPR wavelength matching the emission wavelength of 660 nm. Similarly, the larger Au nanorod has a higher radiative rate enhancement than that of the smaller one at a given LSPR wavelength. The overall UCL enhancement factor F calculated according to Equation (4) for Au nanorods with the diameters of 27.3 and 46.7 nm are shown in Figure 7c,f, respectively. It can be observed that the maximum emission enhancement occurs when the nanorod LSPR wavelength matches the emission wavelength of 660 nm. For the nanorods with the diameter of 27.3 nm, the nanorod with a rod length of 78 nm has a maximum emission enhancement of 29-fold (Figure 7c), while a maximum emission enhancement of 170-fold for the nanorod with a diameter of 46.7 nm and a length of 116 nm is achieved (Figure 7f). This strong enhancement is a combination of an excitation enhancement of 4.2 and a radiative rate enhancement of 40.5. These results clearly indicate that in the presence of Au nanorod not only is a UCNP excited with enhanced intensity, but its emission process is speeded as well. The lifetime measured in the experiment $\tau = 1/(\gamma_r + \gamma_{nr})$, where γ_r and γ_{nr} are the radiative and nonradiative decay rates, respectively. Since the quantum efficiency of the UCNPs is very low (usually <1%), the nonradiative decay rate γ_{nr} dominates the process. Though the radiative rate is enhanced largely as presented in Figure 7, it plays a minor role in the change of the lifetime compared to the nonradiative rate. When the UCNP couples

with Au nanorod, the nonradiative decay rate also increases due to additional nonradiative processes, such as the energy transfer from the UCNP to Au nanorod. Therefore, the shortened lifetime could be observed in the experiment (Figure 6). The larger Au nanorod has a stronger enhancement factor than the smaller one at a given LSPR wavelength due to its larger near-field enhancement at 980 nm and radiative rate enhancements. For the nanorods with a constant diameter, the emission enhancement factor varies dependent on the rod length, which is consistent with the experimental results.

Obviously, the simulated maximum emission enhancement factors are larger than those obtained in experiments. The theoretical simulation was carried out in the ideal conditions, such as uniform light field distribution in the simulation region, an ideal point dipole emitter to replacing UCNPs, a plane wave light source to replacing the laser, probably overstate the maximum emission enhancement factors obtained in the simulations. The imperfect spectral overlap between the scattering spectra of Au nanorods used in experiments and the red emission spectrum of UCNPs is an important contributor. Furthermore, the electric field distribution surrounding the Au nanorod is dependent on the distance, and the average amplified local electric field of Au nanorod in the center of UCNP instead of the actual distance-dependent one is used in the enhancement factor calculation, which also contributes to the above mismatch between the calculated and experimental results.

Here, we demonstrate that the UCL enhancement of UCNPs can be largely improved by increasing the diameter of Au nanorods with a given LSPR wavelength, which mainly originates from the emission and nonresonant excitation enhancement. The resonant excitation coupling as well as the simultaneous resonant emission and excitation coupling of Au nanorods with UCNPs would also be interesting to investigate. But difficulties lie in the synthesis of Au nanorods with longitudinal surface plasmon resonance wavelength matching the 980 nm excitation wavelength on glass slide.

3. Conclusion

Improvement of the UCL enhancement in a single $\text{NaYF}_4:\text{Yb}^{3+}/\text{Er}^{3+}/\text{Mn}^{2+}$ -Au nanorod hybrid dimer is demonstrated by tailoring the scattering and absorption cross-sections of gold nanorods. Au nanorods with the similar longitudinal surface plasmon resonance wavelength but different diameters (27.3 and 46.7 nm), which extinction spectra were dominant by absorption and scattering respectively, were separately assembled with single upconversion nanocrystals by atomic force microscope probe manipulation. UCL enhancement up to 110-fold with larger diameter nanorods were obtained due to stronger scattering ability and greater extent of near-field enhancement. Dark-field and time-resolved rise and decay processes measurements as well as FDTD simulations demonstrate that such strong enhancement includes both the excitation enhancement at the pump wavelength and a significant enhancement of the radiative rate. The enhanced luminescence exhibits a strong dependence on the excitation laser polarization relative to

the nanorod long axis. In the previous work about fluorescence enhancement by gold nanorods, the LSPR wavelength of gold nanorods and the distance between gold nanorods and fluorescence emitters are two commonly considered factors. These results indicate that the diameter of the gold nanorod is also a significant factor to be considered. This work suggests that high scattering/absorption ratio of plasmonic metallic nanoparticles are an important differentiation factor for scattering-based applications such as biolabeling and plasmonic-enhanced spectroscopy.

4. Experimental Section

Nanocrystal Synthesis: Au nanorods were synthesized according to previously reported methods.^[48] The $\text{NaYF}_4:\text{Yb}^{3+}/\text{Er}^{3+}/\text{Mn}^{2+}@\text{SiO}_2$ UCNPs were purchased from Hefei Fluonano Biotech Co., Ltd, China.

Sample Fabrication: UCNPs dispersed in absolute ethyl alcohol were first spin-coated on a clean glass substrate with an average distribution density of $\approx 0.08 \mu\text{m}^{-2}$. Then a drop of dilute aqueous solution of Au nanorods was spin-coated on this glass substrate and dried in vacuum. The controlled nanoassembly of Au nanorods and UCNPs was performed on an AFM (Nanowizard II, JPK Instruments). In detail, as single Au nanorod and single UCNP in proximity were identified, the image mode of the AFM scan software was switched to the manipulation mode. The AFM probe in contact mode was then controlled to move the UCNP along the predetermined line toward to the target Au nanorod. Once the movement was completed, the AFM scan software was switched from the manipulation mode to the image mode, and the UCNP and Au nanorod were reimaged in tapping mode to examine the manipulation result. All these steps were repeated until the UCNP was contacted tightly with one tip of Au nanorod.

Structural and Optical Characterization: Power XRD analysis of the UCNPs was performed on a diffractometer (Bruker D8 ADVANCE, LynxEye detector, operating at 40 kV and 40 mA) at a scanning step of 0.02° in the 2θ range of 10° to 80° (Cu $K\alpha$ radiation, $\lambda = 1.5418 \text{ \AA}$). Transmission electron microscopy images were taken on a JEM-2100F microscopy operating at 120 kV. AFM images were acquired using the above-mentioned AFM operating in tapping mode. Optical absorption spectra were recorded using a UV-vis absorption spectrophotometer. Dark-field imaging and extinction spectra of individual Au nanorods were carried on an Olympus BX51 optical microscope integrated with a camera system: PyloN: $1340 \times 400\text{BRX}$ (Princeton Instruments). A halogen lamp was used as the illumination source. UCL properties of single UCNP and single UCNP-Au nanorod hybrid dimer were investigated in a combined system of a scanning confocal microscope and the AFM.^[45] As illustrated schematically in Figure S1 (Supporting Information), a continuous-wave diode laser at 980 nm was used as the excitation source. Laser power was monitored by a beam sampler and power meter. The excitation laser was linearly polarized, and the polarization direction could be adjusted by a half-wave plate in front of the laser. The laser beam was introduced into an Olympus IX71 inverted microscope with a dichroic mirror and focused on the sample by an oil-immersion objective ($\times 60$, NA = 1.35, UPlanSAPO, Olympus). The resultant UCL from single UCNP was collected by the same microscope objective, and

sent to a single-photon detector based on a silicon avalanche photodiode (APD) for monitoring the UCL intensity or to a spectrometer (SpectraPro-300i, Acton Research Corporation) for spectrum analysis. A short-pass filter cutting off at 780 nm before the APD and spectrometer was used to remove any residual excitation laser signal. UCL spectra were also spatial filtered by a pinhole with the diameter of 75 μm in a telescope system. For time-resolved measurement, the excitation laser was chopped with a repetition rate of 500 Hz by a mechanical chopper (Standford Research SR540). The photons arriving at the ascending and falling edges of the pulse laser were collected as the effective rise and decay lifetime data.

Simulations: Simulations were performed by a commercial software based on the FDTD method (FDTD Solutions, Lumerical Solution, Inc. Canada). The total UCL enhancement includes two processes: excitation enhancement at the pump wavelength and quantum yield enhancement at the emission wavelength. For excitation enhancement simulation, Au nanorod on a thick substrate with a refractive index of 1.47 was illuminated with a total field/scattered field (TFSF) plane wave source ranging from 500 to 1100 nm. The Au dielectric constant was taken from ref. [61], and the refractive index of the surrounding medium was set to be 1.0. A 3D nonuniform meshing was used, and a grid size of 0.5 nm was chosen in the total field domain, with perfectly matched layer (PML) absorption boundary conditions. We also estimated the absorption and scattering cross sections by using a set of power monitors to calculate the net power flowing into the total and scattered field simulation domains, and their sum gave the extinction cross section. The electric field enhancement maps at 660 and 980 nm were evaluated using the frequency domain field profile monitors. To perform the radiative enhancement simulation, the 660 nm emission of SiO₂-coated UCNP with the average diameter of 50 nm could be considered as a two-level system. The radiative enhancement was simulated using the semiclassical approximation, which states that the decay rate for a two-level system at a given location is proportional to the power radiated by a dipole placed at the same location.^[62]

Supporting Information

Supporting Information is available from the Wiley Online Library or from the author.

Acknowledgements

Thanks to Jianmei Chen and Zhiqiang Liang for their assistance with dark-field measurement. This work was funded in part by the National Nature Science Fund of China (11674099, 61378033, and 11621404), Natural Science Foundation of Shanghai (16ZR1409400), Shuguang Program (15SG22), Shanghai International Cooperation Project (16520710600), National Special Funds for the Development of Major Scientific Research Instruments and Equipment (61227902), and the 111 Project (B12024).

Conflict of Interest

The authors declare no conflict of interest.

- [1] J. H. Zeng, J. Su, Z. H. Li, R. X. Yan, Y. D. Li, *Adv. Mater.* **2005**, *17*, 2119.
- [2] H. X. Mai, Y. W. Zhang, R. Si, Z. G. Yan, L. D. Sun, L. P. You, C. H. Yan, *J. Am. Chem. Soc.* **2006**, *128*, 6426.
- [3] F. Wang, Y. Han, C. S. Lim, Y. Lu, J. Wang, J. Xu, H. Y. Chen, C. Zhang, M. H. Hong, X. G. Liu, *Nature* **2010**, *463*, 1061.
- [4] F. Wang, X. G. Liu, *Chem. Soc. Rev.* **2009**, *38*, 976.
- [5] J. Zhou, Q. Liu, W. Feng, Y. Sun, F. Y. Li, *Chem. Rev.* **2015**, *115*, 395.
- [6] D. K. Chatterjee, M. K. Gnanasammandhan, Y. Zhang, *Small* **2010**, *6*, 2781.
- [7] C. Li, D. Yang, P. Ma, Y. Chen, Y. Wu, Z. Hou, Y. Dai, J. Zhao, C. Sui, J. Lin, *Small* **2013**, *9*, 4150.
- [8] N. M. Idris, M. K. Gnanasammandhan, J. Zhang, P. C. Ho, R. Mahendran, Y. Zhang, *Nat. Med.* **2012**, *18*, 1580.
- [9] G. Chen, H. Qiu, P. N. Prasad, X. Chen, *Chem. Rev.* **2014**, *114*, 5161.
- [10] X. Huang, S. Han, W. Huang, X. Liu, *Chem. Soc. Rev.* **2013**, *42*, 173.
- [11] E. Downing, L. Hesselink, J. Ralston, R. Macfarlane, *Science* **1996**, *273*, 1185.
- [12] J. C. Boyer, F. C. J. M. Van Veggel, *Nanoscale* **2010**, *2*, 1417.
- [13] P. Huang, W. Zheng, S. Zhou, D. Tu, Z. Chen, H. Zhu, R. Li, E. Ma, M. Huang, X. Chen, *Angew. Chem. Int. Ed.* **2014**, *53*, 1252.
- [14] F. Wang, R. Deng, J. Wang, Q. X. Wang, Y. Han, H. Zhu, H. X. Zhu, X. Y. Chen, X. G. Liu, *Nat. Mater.* **2011**, *10*, 968.
- [15] J. Wang, R. Deng, M. A. MacDonald, B. L. Chen, J. K. Yuan, F. Wang, D. Z. Chi, T. S. Andy Hor, P. Zheng, G. K. Liu, Y. Han, X. G. Liu, *Nat. Mater.* **2014**, *13*, 157.
- [16] K. Ueno, S. Juodkazis, T. Shibuya, Y. Yokota, V. Mizeikis, K. Sasaki, H. Misawa, *J. Am. Chem. Soc.* **2008**, *130*, 6928.
- [17] B. Wu, K. Ueno, Y. Yokota, K. Sun, H. Zeng, H. Misawa, *J. Phys. Chem. Lett.* **2012**, *3*, 1443.
- [18] K. T. Shimizu, W. K. Woo, B. R. Fisher, H. J. Eisler, M. G. Bawendi, *Phys. Rev. Lett.* **2002**, *89*, 117401.
- [19] M. Song, B. Wu, G. Chen, Y. Liu, X. Ci, E. Wu, H. Zeng, *J. Phys. Chem. C* **2014**, *118*, 8514.
- [20] Y. Fu, J. Zhang, J. R. Lakowicz, *J. Am. Chem. Soc.* **2010**, *132*, 5540.
- [21] S. Khatua, P. M. Paulo, H. Yuan, A. Gupta, P. Zijlstra, M. Orrit, *ACS Nano* **2014**, *8*, 4440.
- [22] C. Ayala-Orozco, J. G. Liu, M. W. Knight, Y. Wang, J. K. Day, P. Nordlander, N. J. Halas, *Nano Lett.* **2014**, *14*, 2926.
- [23] S. Schietinger, T. Aichele, H. Q. Wang, T. Nann, O. Benson, *Nano Lett.* **2009**, *10*, 134.
- [24] M. Saboktakin, X. Ye, S. J. Oh, S. H. Hong, A. T. Fafarman, U. K. Chettiar, C. R. Kagan, *ACS Nano* **2012**, *6*, 8758.
- [25] N. J. Greybush, M. Saboktakin, X. Ye, C. Della Giovampaola, S. J. Oh, N. E. Berry, C. R. Kagan, *ACS Nano* **2014**, *8*, 9482.
- [26] Q. Zhan, X. Zhang, Y. Zhao, J. Liu, S. He, *Laser Photonics Rev.* **2015**, *9*, 479.
- [27] A. L. Feng, M. L. You, L. Tian, S. Singamaneni, M. Liu, Z. Duan, T. Lu, F. Xu, M. Lin, *Sci. Rep.* **2015**, *5*, 7779.
- [28] Z. Yin, D. Zhou, W. Xu, S. Cui, X. Chen, H. Wang, S. Xu, H. Song, *ACS Appl. Mater. Interfaces* **2016**, *8*, 11667.
- [29] Z. Yin, H. Li, W. Xu, S. Cui, D. Zhou, X. Chen, Y. Zhu, G. Qin, H. Song, *Adv. Mater.* **2016**, *28*, 2518.
- [30] P. Kannan, F. A. Rahim, R. Chen, X. Teng, L. Huang, H. Sun, D.-H. Kim, *ACS Appl. Mater. Interfaces* **2013**, *5*, 5508.
- [31] A. L. Feng, M. Lin, L. Tian, H. Y. Zhu, H. Guo, S. Singamaneni, Z. Duan, T. J. Lu, F. Xu, *RSC Adv.* **2015**, *5*, 76825.
- [32] H. Huang, F. Rosei, F. Vetrone, *Nanoscale* **2015**, *7*, 5178.

- [33] X. Wu, L. Xu, W. Ma, L. Liu, H. Kuang, N. A. Kotov, C. Xu, *Adv. Mater.* **2016**, *28*, 5907.
- [34] W. Zhang, F. Ding, S. Y. Chou, *Adv. Mater.* **2012**, *24*, OP236.
- [35] M. Saboktakin, X. Ye, U. K. Chettiar, N. Engheta, C. B. Murray, C. R. Kagan, *ACS Nano* **2013**, *7*, 7186.
- [36] Q. C. Sun, H. Mandoor, J. C. Ribot, V. Singh, I. I. Smalyukh, P. Nagpal, *Nano Lett.* **2014**, *14*, 101.
- [37] D. Lu, S. K. Cho, S. Ahn, L. Brun, C. J. Summers, W. Park, *ACS Nano* **2014**, *8*, 7780.
- [38] X. Chen, W. Xu, L. Zhang, X. Bai, S. Cui, D. Zhou, Z. Yin, H. Song, D.-H. Kim, *Adv. Funct. Mater.* **2015**, *25*, 5462.
- [39] A. Li, M. Lü, L. Guo, Z. Sun, *Small* **2016**, *12*, 2092.
- [40] H. Zhang, Y. Li, I. A. Ivanov, Y. Qu, Y. Huang, X. Duan, *Angew. Chem.* **2010**, *122*, 2927; *Angew. Chem. Int. Ed.* **2010**, *49*, 2865.
- [41] P. Yuan, Y. H. Lee, M. K. Gnanasammandhan, Z. Guan, Y. Zhang, Q. H. Xu, *Nanoscale* **2012**, *4*, 5132.
- [42] M. Fujii, T. Nakano, K. Imakita, S. Hayashi, *J. Phys. Chem. C* **2013**, *117*, 1113.
- [43] J. M. Liu, Y. Y. Liu, D. D. Zhang, G. Z. Fang, S. Wang, *ACS Appl. Mater. Interfaces* **2016**, *8*, 29939.
- [44] N. Mauser, D. Piatkowski, T. Mancabelli, M. Nyk, S. Mackowski, A. Hartschuh, *ACS Nano* **2015**, *9*, 3617.
- [45] G. Chen, C. Ding, E. Wu, B. Wu, P. Chen, X. Ci, Y. Liu, J. Qiu, H. Zeng, *J. Phys. Chem. C* **2015**, *119*, 22604.
- [46] B. Nikoobakht, M. A. El-Sayed, *Chem. Mater.* **2003**, *15*, 1957.
- [47] W. Ni, X. Kou, Z. Yang, J. Wang, *ACS Nano* **2008**, *2*, 677.
- [48] X. Ye, C. Zheng, J. Chen, Y. Gao, C. B. Murray, *Nano Lett.* **2013**, *13*, 765.
- [49] N. J. Durr, T. Larson, D. K. Smith, B. A. Korgel, K. Sokolov, A. Ben-Yakar, *Nano Lett.* **2007**, *7*, 941.
- [50] J. Wang, G. Zhu, M. You, E. Song, M. I. Shukoor, K. Zhang, M. B. Altman, Y. Chen, Z. Zhu, C. Z. Huang, W. Tan, *ACS Nano* **2012**, *6*, 5070.
- [51] W. S. Kuo, C. N. Chang, Y. T. Chang, M. H. Yang, Y. H. Chien, S. J. Chen, C. S. Yeh, *Angew. Chem.* **2010**, *122*, 2771; *Angew. Chem. Int. Ed.* **2010**, *49*, 2711.
- [52] Q. Su, S. Han, X. Xie, H. Zhu, H. Chen, C. K. Chen, R. S. Liu, X. Chen, F. Wang, X. Liu, *J. Am. Chem. Soc.* **2012**, *134*, 20849.
- [53] F. Zhang, R. Che, X. Li, C. Yao, J. Yang, D. Shen, P. Hu, W. Li, D. Zhao, *Nano Lett.* **2012**, *12*, 2852.
- [54] G. Tian, Z. Gu, L. Zhou, W. Yin, X. Liu, L. Yan, S. Jin, W. Ren, G. Xing, S. Li, Y. Zhao, *Adv. Mater.* **2012**, *24*, 1226.
- [55] J. Mock, D. R. Smith, S. Schultz, *Nano Lett.* **2003**, *3*, 485.
- [56] S. Kim, D. C. Ratchford, X. Li, *ACS Nano* **2009**, *3*, 2989.
- [57] G. Lu, Y. Wang, R. Y. Chou, H. Shen, Y. He, Y. Cheng, Q. Gong, *Laser Photonics Rev.* **2015**, *9*, 530.
- [58] P. Reineck, D. Gómez, S. H. Ng, M. Karg, T. Bell, P. Mulvaney, U. Bach, *ACS Nano* **2013**, *7*, 6636.
- [59] R. Chhabra, J. Sharma, H. Wang, S. Zou, S. Lin, H. Yan, Y. Liu, *Nanotechnology* **2009**, *20*, 485201.
- [60] C. S. Yun, A. Javier, T. Jennings, M. Fisher, S. Hira, S. Peterson, B. Hopkins, N. O. Reich, G. F. Strouse, *J. Am. Chem. Soc.* **2005**, *127*, 3115.
- [61] E. Palik, *Handbook of Optical Constants of Solids*, Academic Press, New York **1984**.
- [62] L. Novotny, B. Hecht, *Principles of Nano-Optics*, Cambridge University Press, New York **2006**.

Received: April 10, 2017
Revised: June 13, 2017
Published online: August 7, 2017